SINTERING BEHAVIOR AND KINETIC EVALUATION OF HYDROXYAPATITE BIO-CERAMICS FROM BOVINE BONE

ZHANG XUEBIN, DING YUNFEI, WANG SONGLIN*, XU JIE, FENG YI

School of Materials Science & Engineering, Hefei University of Technology, Hefei 230009, P.R. China
** Tongling University, Tongling 244000, P.R. China*

E-mail: zzhhxxbb@126.com

Submitted November 30, 2009; accepted April 27, 2010

Keywords: Hydroxyapatite, Bio-ceramics, Bovine bone, Sintering kinetics

The Sintering behavior and kinetic evaluation of the bio-ceramics from bovine bone are investigated by stepwise isothermal dilatometry (SID), X-ray diffraction (XRD) and scanning electron microscope (SEM). The isothermal shrinkage data obtained from SID could be well analyzed to get kinetic parameters according to the empirical rate equation developed by Makipirtti-Meng, $dY/dt = nk(T)Y(1-Y)[Y/(1-Y)]^{1/n}$, where Y is the fractional volume shrinkage during sintering process and n a dimensionless exponent. The apparent activation energy ΔE values obtained for 1000-1100°C and 1100-1250°C are 84.1 and 52.8 kJ/mol, respectively. Correspondingly, the exponent n that can be served to reveal the morphology changing during the sintering process are also much different in the two temperature ranges, which is well consistent with the SEM observation.

INTRODUCTION

Hydroxyapatite (HA), is being widely utilized in the medical applications in both orthopeadics and dentistry, especially as a bone substitute material, due to the good biocompatibility, bioactivity and other properties [1,2]. Many ways have been found to synthesize HA. However, the synthesis processes might be either complicated or biologically unsafe, and the synthesized HA does not have adequate biological properties as the natural apatite existing in the bones [3]. Recently natural HA are produced from natural resources, such as bovine bones [4], teeth [5] and corals or nacreous material [6]. These methods are economically, environmentally preferable and biologically safe.

Commonly, HA is used as a bio-ceramic either in the form of dense sintered parts or of powder. As to the former, the sintering is of prime importance because it controls the micro-structure, phase and the mechanical character of the ceramics. Some researches on the sintering of bio-ceramics from the synthesized HA have been reported. The sintering activation energies were calculated from the Arrhennius plots of the variation of the grain size [7, 8] or the length [1,9] or the specific surface area [10,11] as function of the sintering temperature.

However, the microstructure development and the formation kinetics of the HA ceramics from natural resources have seldom been reported in the literatures. There would be some similar behavior in the formation kinetics of bio-ceramics from the natural materials mentioned above. Considering these reasons, the topic of sintering kinetics of bio-ceramic from bovine bone presented in this paper is of great significance.

On the other hand, the methods used on synthesized HA reported before [1,7-11] to do this kind of work have some apparent drawbacks:

1. The sintering process is neither a one-dimensional shrinkage (the grain size or the length), nor a two-dimensional shrinkage (the surface area), instead it is a bulk shrinkage, i.e., a three-dimensional transformation process.
2. The variation data for each temperature points of length, grain size and specific surface area were determined in room temperature after sintering, which is inconvenient, and the data are not real-time accurate for the variation between high and room temperature.

Actually, the rate process data can be readily taken by measuring the specimen length during heating with time in a dilatometer. The problem is how to analyze the data to get the desired information.

The empirical rate equation developed by Makipirtti-Meng could be used to analyze the isothermal shrinkage data from SID, which has been used in the sintering processes for Y-TZP [12], Al_2O_3[13], mullite [14] and natural diatomite [15] with fair success.

The equation to describe "dynamic" relative volumetric shrinkage with holding time, as follows:

$$\frac{dY}{dt} = nk(T)Y(1-Y)\left(\frac{Y}{1-Y}\right)^{\frac{1}{n}} \quad (1)$$

With the correct concept for fractional transformation and assuming isotropic sintering, the dynamic real-time fractional densification Y is defined as

$$Y = \frac{V_0 - V_t}{V_0 - V_f} = \frac{L_0^3 - L_t^3}{L_0^3 - L_f^3} \quad (2)$$

where $V_0(L_0)$, $V_t(L_t)$, and $V_f(L_f)$ are the initial volume (length), volume (length) at time t, and the fully dense volume (length) of the specimen, respectively. The $k(T)$ in Equation (4) is the specific rate constant, which is related to temperature following the Arrhenius law:

$$k(T) = k_0 \exp(-\Delta E / kT) \quad (3)$$

where k_0 is the frequency factor and ΔE is the apparent activation energy of the sintering process.

In this work, we present the research of the sintering formation kinetics of bio-ceramics from bovine bone employing the SID associated with other characterization tools.

EXPERIMENTAL

Preparation of the specimens

The naturally derived HA powder used in this study was originated from bovine bones. The bones were calcined at 700°C for 4 h to completely remove organics. The starting powders were obtained by milling the calcined bones in planetary ball mill (QM-3SP2, Nanjing University Instrument Plant, China) at speed of 400r/min for 16 h.

The green bar specimens with dimensions of 5 mm × 5 mm × 30 mm were prepared by die-pressing under the pressure of 130 MPa. Some of them were sintered and the others were used to obtain the SID shrinkage data. The sintering was performed in a programmable HT furnace (Nabertherm, Bremerhaven, Germany) in air at a ramping rate of 3°C/min up to 600°C, followed by 5°C/min to various temperatures (750°C-1250°C). Then the specimens were soaked for 2 h and cooled down to room temperature naturally.

Characterization of the specimens

XRD patterns of the sintered specimens were obtained by XRD diffraction unit (Shimadzu XRD-600, Japan) with Cu$K\alpha$ radiation generated at 40 kV and 40 mA, in the $20° < 2\theta < 60°$ range at a scan speed of 2°/min. The phases were determined by comparing the patterns with JCPDS standards.

The microstructures of the specimens were observed using scanning electron microscope (SEM) (Jeol, Japan).

Stepwise isothermal dilatometry measurement

The shrinkage behavior of green specimens was carried out by a horizontal Dilatometer (DIL 4021C). The shrinkage was measured in the axial direction with a linear variable differential transducer (sensitivity is smaller than 0.1μ m) and the pressure added to the sample by dilatometer was minimized to 0.2 N so that accurate shrinkage data could be obtained. The temperature was measured using a calibrated thermocouple, which was placed directly above the sample.

A special program was operated to perform an SID measurement. Time (s), temperature (°C), and length shrinkage (mm) data were recorded automatically. The SID program was as follows: the temperature holding steps were 1000, 1050, 1100, 1150, 1200 and 1250°C for 30 min, respectively, and all of the ramping rates between the isothermal holdings are 10°C/min.

Analysis the SID experimental data by equation (3)

Firstly, we plot $\ln\{(dY/dt)[1/Y(1-Y)]\}$ versus $\ln[(1-Y)/Y]$, where Y can be calculated from Equation (2) as L_0, L_t, and L_f are all experimentally determined. The plot in the form of a straight line means the equation is well valid to the case process, see Equation (4) logarithmic transformed from Equation (2).

$$Ln\left[\frac{dY}{dt}\cdot\frac{1}{Y(1-Y)}\right] = Ln[nk(T)] + \frac{1}{n}Ln\left(\frac{Y}{1-Y}\right) \quad (4)$$

The process parameters, n and $k(T)$, are then achieved from the slope and intercept, respectively. The data of rate constant $k(T)$ obtained at various temperatures are then plotted and linearly fitted according to the Arrhenius law to get k_0 and ΔE values.

RESULTS AND DISCUSSION

Phase identification and microstructure observation

Figure 1 presents the XRD patterns of bio-ceramics from bovine bone annealed at varying temperatures.

The XRD analysis of the five calcined samples revealed mainly a phase of HA, with the peaks matching JCPDS standards (9-432). The XRD signatures of bone annealed at 750°C and 1000°C were almost similar and exhibited a substantial increase in peak height and a decrease in peak width, thus indicating an increase in crystallinity and crystallite size.

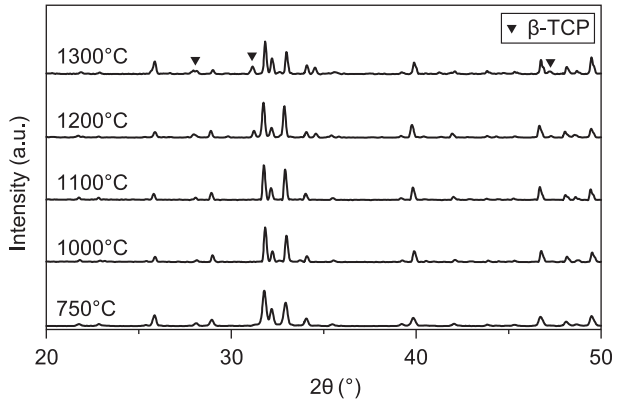

Figure 1. The XRD for annealed bovine bone powders and bioceramic sintered at different temperature (Key: ▼ = β-TCP).

However, annealing above 1000°C resulted in partial decomposition of the HA phase to form minor calcium phosphate phase of β-TCP. As the annealing temperature increased to 1100°C, the intensity of the characterized peaks for β-TCP, which is located at 2θ angles of 27.78, 31.18 and 47.78 was observed to gradually increase. The present XRD results suggest that the sintering of the ceramics from bovine bone below 1100°C is a simple uniphase sintering of HA. And above 1100°C, the annealing process included the physical sintering of be two phases (HA and β-TCP) and the chemical decomposition of HA, which was more complex.

Figure 2 shows SEM microphotographs of samples calcined at different temperatures. It can be seen that the microstructure below 1100°C has many through micropores distributed on the body. When the temperature is higher than 1250°C, the microstructure varies apparently. The initial HA particles are converted into an integral body, and the through micro-pores become closed. When soaked at 1150°C, although there still many through pore, the microstructure had started change, as could be seen in the Figure 2b.

Kinetic analysis based on SID measurement using the Makipirtti-Meng model

The initial length of the green HA bar used for SID measurement was 11.400 mm. The plots of the relative length shrinkage (%) as well as operating step isothermal temperature (°C) versus time (min) are presented in Figure 3. According to Equation (4), the relevant data in Figure 3 were transferred to plots of $\ln\{(dY/dt)[1/Y(1-Y)]\}$ versus $\ln[(1-Y)/Y]$ (Figure 4). A very fine linear relationship can be seen in every segment of an isothermal holding. From the slopes and intercepts ($\ln[nK(T)]$) of the straight lines, the values of time exponent n and $\ln k(T)$ as well as the correlation factor R for linear fitting are calculated and listed in Table1. The fact that R values are close to one proves that the Makipirtti-Meng equation agrees very well with the sintering shrinkage data of this system.

Figure 5 presents plots of n versus $1000/T$ based on the data from Table 1. The plot consists of two steps with different increase rate according to the sintering temperature. The turning point is at about 1100°C. In first step, the n values increase slowly from a very small value 0.2106 for 1000°C to 0.2907 for 1100°C, which imply that the microstructure is changing simple but are still far from unit, indicating the complex microstructure characterized by fractal morphology ($n < 1$).

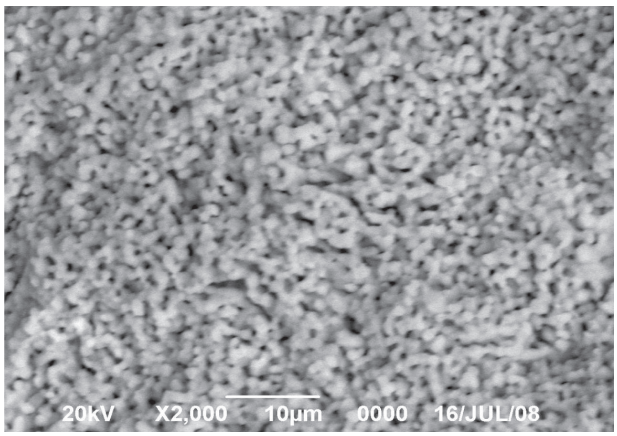

a)

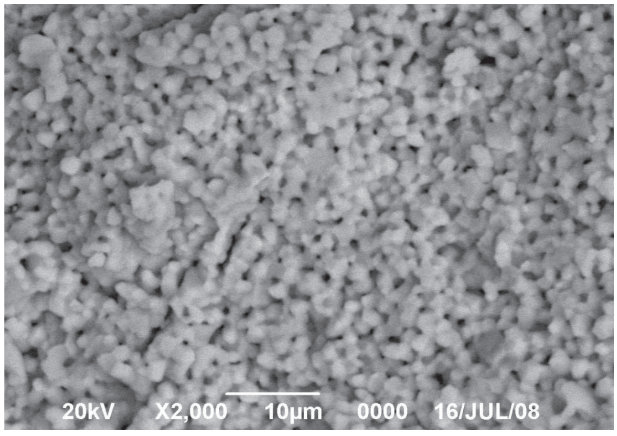

b)

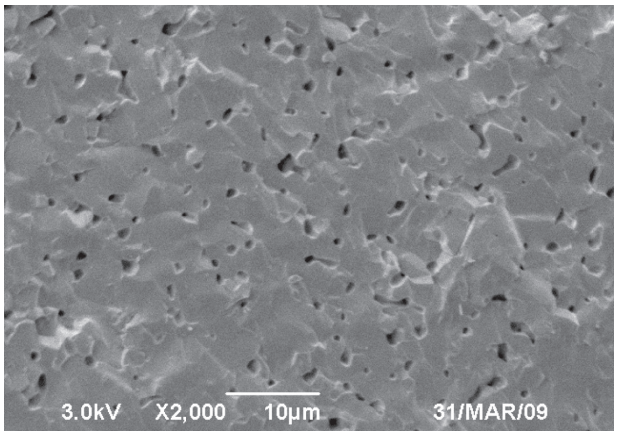

c)

Figure 2. Influence of sintering temperature on the microstructure - a) 1100°C, b) 1150°C, c) 1250°C).

For temperatures 1150°C and 1250°C the *n* values are, respectively, 0.4166 and 0.6254, which indicate a simpler morphology to attribute a mass diffusion transfer and sintering shrinkage. And the change is quicker than that in first step. These results are very consistent with the SEM observation mentioned previously (see Figure 2).

Figure 6 presents plots of ln*k(T)* versus 1000/*T* based on the data from Table 1. The specific rate constant *k(T)* for the sintering shrinkage is assumed to follow the Arrhenius law as Equation (3). The plot consists of two straight lines with different slopes, implying different shrinkage mechanisms in two temperature ranges. The turning point of ln*k(T)* is also at about 1100°C. The process activation energies (ΔE) are calculated from the slopes to be 84.1 and 52.8kJ/mol, respectively, which should correspond to the activation energy for diffusion in HA.

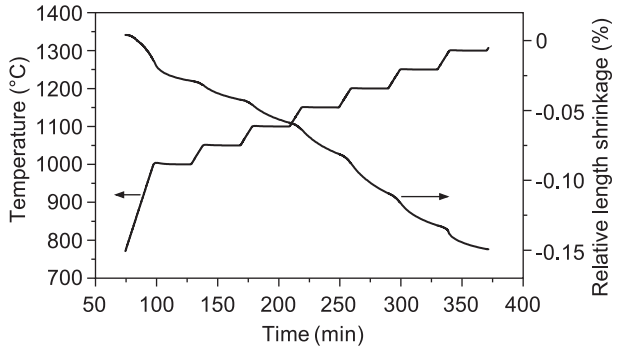

Figure 3. Stepwise isothermal dilatometry shrinkage curve of the green compact of HA.

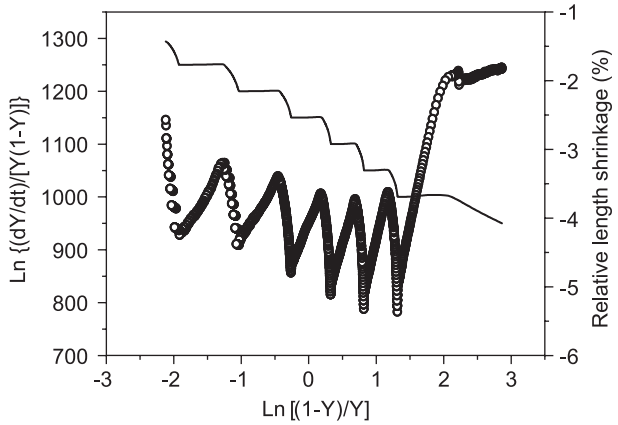

Figure 4. Plots of ln{(dY/dt)[1/Y(1-Y)]} versus ln[(1-Y)/Y] according to Equation (8).

The activation energy value for higher isothermal temperature (52.8kJ/mol), is in agreement with the values reported by other researchers, e.g. 47 kcal/mol [8], 56 kcal/mol [16], 57 kcal/mol [17] and 58 kcal/mol [7] for synthetic HA. However, none of these reported work divided the whole sintering process into two steps, and the value in this paper from bovine bone for low temperature (84.1/mol) is fairly higher than those reported ones from the synthetic HA. These discrepancies could

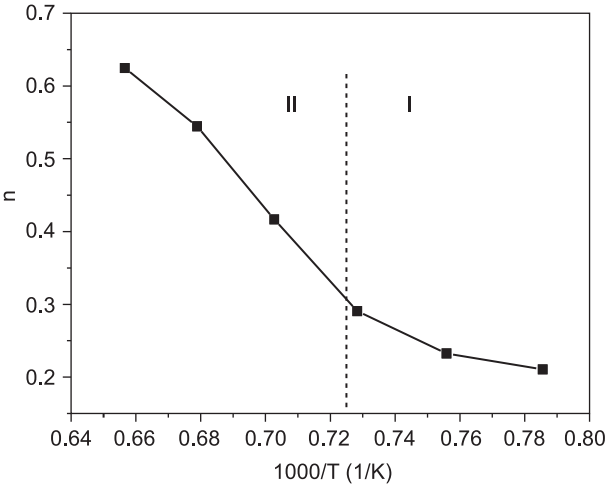

Figure 5. Plots of lnk(T) versus 1000/T based on the data in Table 1.

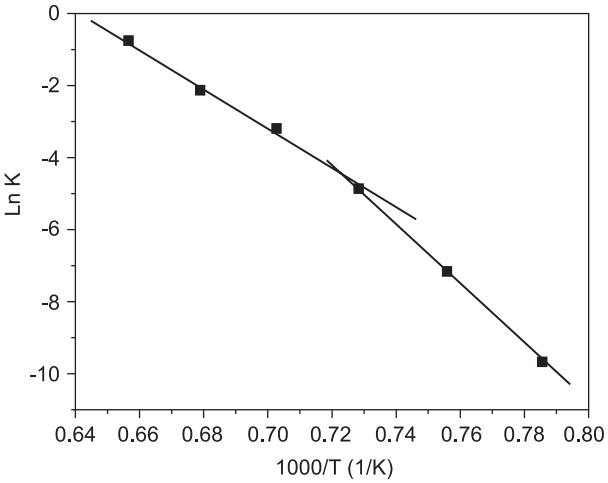

Figure 6. Plots of lnk(T) versus 1000/T based on the data in Table 1.

Table 1. Kinetic analyses of SID data according to Makipirtti-Meng equation.

T (°C)	1000/*T* (K^{-1})	ln[n*K*(*t*)]	1/*n*	*n*	ln*k*	*R*
1250	0.657	-1.2252	1.6014	0.6245	-0.7543	0.9908
1200	0.679	-2.6489	1.8365	0.5445	-2.1296	0.9420
1150	0.703	-4.0699	2.4001	0.4166	-3.1944	0.9993
1100	0.728	-6.099	3.4398	0.2907	-4.864	0.9996
1050	0.756	-8.6199	4.3017	0.2325	-7.1608	0.9999
1000	0.786	-11.232	4.7487	0.2106	-9.6741	0.9996

be attributed mainly to the different starting HA powder used and the methods of analysis and testing employed.

The rather high ΔE value for temperature below 1100°C (84.1 kJ/mol) indicates a high energy barrier associated with the shrinkage process at this stage. It is commonly recognized that the first stage of sintering at lower temperatures involves more complicated processes such as sintering within agglomerated particles driven by decrease in surface area and the neck-formation between particles through both reactions and surface diffusion. In this case, crystalline HA formation from amorphous materials (See XRD for 750°C in Figure 1), neck-formation of porous ceramics, and normal sintering process may be expected. Therefore, the apparent activation energy should be rather large compared with the process of sintering. Correspondingly, the time exponent n values are usually quite smaller, 0.2106-0.2907 in this work as mentioned above, revealing the very complicated microstructure morphology.

The lower activation energy at second sintering step may caused by the simpler morphology to attribute a mass diffusion transfer and sintering shrinkage corresponding to the time exponent *n* values from 0.4166 for 1150°C to 0.6254 for 1250°C.

CONCLUSION

The Sintering behavior and kinetic evaluation of bio-ceramics from natural bovine bone were investigated by SID, XRD phase identification and SEM observation.

The Makipirtti-Meng model was proved to be of great service in the analysis of SID data to get kinetic parameters of the HA bio-ceramic from bovine bone. For the formation temperature range (1000-1250°C), the sintering shrinkage shown different kinetic behaviors below and above 1100°C. The activation energies were 84.1 and 52.8 kJ/mol, respectively. The rather small exponent *n* values (0.2106-0.2907) and high activation energy for lower temperature revealed the complexity in the process and microstructure, while the higher *n* values (0.654 and 0.764) for 1100-1250°C and smaller activation energy described a simpler morphology of the ceramic being formed, which was consistent with the SEM observation.

Acknowledgement

The authors acknowledge the Ministry of Education of China for financial support, under Contract No. 20070359034.

References

1. Landi E., Tampieri A., Celotti G., Sprio S.: Journal of the European Ceramic Society *20*, 2377 (2000).
2. Junguo Li, Toshiyuki Hashida: J. Mater. Sci. *42*, 5013 (2007).
3. Nasser A. M. Barakat, Myung Seob Khil, A. M. Omran: Journal of materials processing technology *209*, 3408 (2009).
4. Joschek S., Nies B., Krotz R., Gopferich A.: Biomaterials *21*, 1645 (2000).
5. Xiaoying L., Yongbin F., Dachun G., Wei C.: Key Eng. Mater. *342*, 213 (2007).
6. Lemos A. F., Rocha J. H. G., Quaresma S.S.F., Kannan S.: Journal of the European Ceramic Society *26*, 3639 (2006).
7. Muralithran G., Ramesh S.: Ceramics International. *26*, 221 (2000).
8. Van landuyt P., Li F., Keustermans J. P., Streydio J. M., Delannay F.: J.Mater.Sci: Mater Med. *6*, 8 (1995).
9. Jokanovic V., Jokanovic B., Markovic D., Zivojinovic V.: Materials Chemistry and Physics *111*, 180 (2008).
10. Bernache-Assollant D., Ababou A., Champion E., Heughebaert M.: Journal of the European Ceramic Society *23*, 229 (2003).
11. Bailliez S., Nzihou A.: Chemical Engineering *98*, 141 (2004).
12. Meng G. Y., Sorensen O.T.: *Advanced Structural Materials*, 2nd ed., p.369–374, Elsevier Science Publishers B. V., Amsterdam 1991.
13. Wang H. T., Liu X. Q., Chen F. L., Meng G. Y.: J.Am. Ceram.Soc. *81*, 781 (1998).
14. Liu Y. F., Liu X. Q., W. Tao S., Meng G. Y., Sorensen O. T.: Ceram.Int. *28*, 479 (2002).
15. Xuebin Zhang, Xingqin Liu, Guangyao Meng: J.Am. Ceram.Soc. *88*, 1826 (2005).
16. Jarcho M., Bolen C. H., Thomas M. B., Bobick J., Kay F., Doremus R.H.: J. Mater. Sci. *11*, 2027 (1976).
17. Kamiya K., Yoko T., Tanaka K., Fujiyama Y.: J. Mater. Sci. *24*, 827 (1989).